Available online at www.sciencedirect.com
ScienceDirect
Icarus 195 (2008) 674–685
ICARUS
www.elsevier.com/locate/icarus

Asteroid exosphere: A simulation for the ROSETTA flyby targets (2867) Steins and (21) Lutetia

B. Schläppi *, K. Altwegg, P. Wurz

Physikalisches Institut, Universität Bern, Sidlerstrasse 5, CH-3012 Bern, Switzerland

Received 12 July 2007; revised 20 December 2007

Available online 12 January 2008

Abstract

Asteroids (2867) Steins and (21) Lutetia are two flyby targets of ESA's cornerstone mission Rosetta. Since Rosetta is a cometary mission, some of the instruments are designed to investigate the surroundings of small bodies. To prepare the operation of these instruments, in our case the ROSINA instrument, for the asteroid flyby's, we adapted a Monte Carlo simulation code, initially developed to simulate the exosphere of Mercury. Modelled release processes are solar wind sputtering, micrometeorite impact vaporisation, photon stimulated desorption and in some cases thermal release. Released species were derived from estimations of the asteroid composition. This was done for both asteroids by using results from ground based observations and meteorite science. We used the estimated compositions and other known properties as input for the simulation. Our results suggest that neutral sodium and oxygen might be the best species to investigate by the means of mass spectrometry: We expect to be able to detect these species at least in the exosphere of (21) Lutetia.

Keywords: Asteroids, composition

1. Introduction

Rosetta, a cornerstone mission of the European Space Agency (ESA), will investigate the coma and the nucleus of Comet 67P/Churyumov–Gerasimenko while the comet is approaching the Sun. On its long way to the comet, the Rosetta spacecraft will flyby two main belt asteroids, (2867) Steins and (21) Lutetia.

Rosetta, being above all a comet mission and equipped with instruments for that purpose, may reveal some new information about these asteroids: The Rosetta Orbiter Spectrometer for Ion and Neutral Analysis (ROSINA) will be used to investigate the exospheres of these bodies.

Here we report on the results of a Monte Carlo code, originally developed for Mercury (Wurz and Lammer, 2003; Wurz et al., 2007), now being extended to the two flyby targets of Rosetta. Because of their relatively small size, asteroids are not able to retain a thicker atmosphere than Mercury, which has a pressure at the surface of about 10^{-10} mbar, given from the Mariner 10 investigations (Hunten et al., 1988). Because the outgassing is very small for most asteroids, the atmospheres will be free of collisions between released particles and the exobase will coincide with the asteroid surface. Mercury shows a similar behaviour and therefore the adaptation of the code is reasonable and straight forward.

The initial goal of this work was to investigate if measurements of asteroid exospheres are possible with in situ mass spectrometers, namely ROSINA, and what species would yield the best chances for a successful detection.

2. Simulation code

The two-dimensional Monte Carlo code assumes angular and velocity distributions for each release process and then tracks the trajectory of each released particle through the exosphere until the particle either escapes or hits the surface of the asteroid. Splitting up the velocity vector into a perpendicular (z axis) and two parallel components relative to the surface plane, the elevation angle is given. The code uses an altitude step in z direction to derive the flight time t for each step. Af-

* Corresponding author. Fax: +41 31 631 44 05.
E-mail address: schlaeppi@space.unibe.ch (B. Schläppi).

0019-1035/$ – see front matter
doi:10.1016/j.icarus.2007.12.021

ter the time t, the elevation angle and the velocity component in z direction change due to the gravitation of the body. The new values for these properties are calculated and used to derive the next step. The model does not take radiation pressure into account.

By counting how many particles reach a certain altitude, a density profile for each species and release process is derived. Scaling the calculated density profile with a column or surface density gives the vertical density structure of the exosphere. Using known column or surface densities, the simulation showed good results for the H, He and Ca contribution of Mercury's exosphere (Wurz and Lammer, 2003). Recently, the code was extended to calculate the exospheric density of a species at the surface from the surface density of the solid and the release process (Wurz et al., 2007).

For the two asteroids, neither column nor surface densities are known from observations. Therefore we have to calculate the exospheric surface density, N_i. The surface density N_i for a species i of one particular release process is

$$N_i = \frac{\varphi_i}{v_i}, \tag{1}$$

with φ_i the flux of this species released by the chosen process and v_i the average release velocity of particles by this process, which can be derived from the velocity or energy distribution used to simulate the initial conditions of each particle. φ_i depends on the mechanism that effectively gives a particle enough energy to escape from the surface.

To release particles from the asteroid surface, four different release processes are simulated:

Thermal release: The surface temperature is the reason for diffusion and release of volatiles to the exosphere. Although not as important as on active comets, this process is responsible for the release of water or implanted solar wind ions (for instance He) into an asteroid exosphere. A Maxwellian distribution is used to determine the mean velocity of thermally released particles. The forcing temperature in this case is the surface temperature, which follows roughly a $T_{ss} \cdot \cos^{1/4}(\alpha)$ law, with T_{ss} the temperature at the subsolar point at the dayside and α the angular distance to the subsolar point. The subsolar temperature T_{ss} for asteroids can be calculated as

$$T_{ss} = \left(\frac{(1-A_b)S}{\eta\varepsilon\sigma}\right), \tag{2}$$

where A_b is the bolometric bond albedo, S the solar constant scaled to the heliocentric distance at the encounter, η is the beaming factor, ε the emissivity, and σ the Stefan–Boltzmann constant.

The angular distribution of the velocity vectors are constructed by a set of three Gaussian deviates. The initial particle velocity components are then given by the typical thermal velocity scaled with the three deviates and an additional offset, coming from the rotation of the asteroid. If thermal release occurs at all for asteroids, the flux $\varphi_i^{\text{thermal}}$ of a certain species is dependent on the composition, in particular of the abundance of volatiles at the surface and must therefore be estimated individually.

Particle sputtering occurs when solar wind ions hit the surface and act as sputter agents. All elements present at the surface are introduced to the exosphere of an asteroid by sputtering. The released particle flux depends on the solar wind flux φ_{sw_i}, the total sputter yield Y, which gives the number of released particles per incident ion (typically 0.1 for solar wind ions), and the relative abundance F_i of the investigated species i in the asteroid regolith. Using estimated compositions together with a TRIM.SP (Biersack and Eckstein, 1984; Ziegler, 2004) simulation, we have sputter yields Y_i for each species

$$\varphi_i^{\text{sputter}} = \varphi_{\text{sw}} Y F_i = \varphi_{\text{sw}} Y_i. \tag{3}$$

To obtain the sputter yields with the TRIM.SP software we follow the procedure described in detail by Wurz et al. (2007). The exosphere produced through sputtering represents more or less the surface composition on an atomic level. Although asteroids may posses intrinsic magnetic fields (e.g. Richter et al., 2001) and meteorites often show magnetisation, we assume that a possible deflection of the solar wind ions is negligible and sputtering occurs on the entire day side of the asteroid.

From the energy distribution (Wurz and Lammer, 2003 and references therein)

$$f(E_e) = \frac{6E_b}{3-8\sqrt{\frac{E_b}{E_c}}} \frac{E_e}{(E_e+E_b)^3}\left(1-\sqrt{\frac{E_e+E_b}{E_c}}\right) \tag{4}$$

a mean release velocity for sputtered particles was derived. In the energy distribution E_e is the energy of the sputtered particle, E_b the binding energy of the particle on the surface (typically some eV) and E_c the cut off energy, given by the maximum energy that can be transferred from a solar wind ion to the sputtered particle.

For the azimuth angle a uniform distribution over 2π is used, and for the polar angle δ a $\cos^n(\delta)$ function can be used in general for sputtering. n depends on the structure of the surface and equals 1 for a porous regolith (Cassidy and Johnson, 2005).

Photon stimulated desorption (PSD) occurs only for volatile species like Na, K and maybe S and water. These species must be replenished at the surface by some process from beneath. Impacting micrometeorites or chemical sputtering induced by solar wind protons, for instance, could be sources of these volatiles. Diffusion to the surface would then expose the particles to the solar UV photons. PSD may be responsible for the main Na exosphere of Mercury and there is no reason why this process should not occur on asteroids as well. The dominant ejecta of photon stimulated desorption are neutral Na and K (Killen and Ip, 1999).

The flux of Na atoms $\varphi_{\text{Na}}^{\text{PSD}}$ released via PSD is given by (Wurz and Lammer, 2003)

$$\varphi_{\text{Na}}^{\text{PSD}} \approx \frac{1}{4}\varphi_{\text{photon}} Q_{\text{Na}} F_i N_S, \tag{5}$$

where Q_{Na} is the PSD cross-section [(1–3) $\times 10^{-20}$ cm^2] for wavelengths between 400 and 250 nm. φ_{photon} is the flux of photons per unit area and time, which is, integrated over the

wavelength range of 0.1–318.0 nm, in the orbit of Earth 3.31×10^{15} cm^{-2} s^{-1}. N_S is the regolith surface density, assumed to be 7.5×10^{14} cm^{-2}, the same value Wurz and Lammer (2003) used in their calculation.

F_i is the fraction of species i in the regolith. We use the same PSD cross section also for the other species released via PSD. The energy distribution used for the simulation is (Wurz and Lammer, 2003 and references therein)

$$f_{\mathrm{PSD}}(E) = \beta(1+\beta)\frac{EU^{\beta}}{(E+U)^{2+\beta}}; \tag{6}$$

here E is the particle energy, U the characteristic energy for PSD and β is a shape parameter of the distribution, which is species dependent ($\beta_{\mathrm{Na}} = 0.7$, $\beta_K = 0.25$). For U we use, following Wurz and Lammer (2003), energies derived from temperatures 600 and 400 K above the surface temperature for Na and K, respectively. The angular distributions for PSD are the same as for solar wind sputtering, except for the power factor n for the polar angle distribution: For PSD we used $n = 2$.

Micrometeorite impact vaporisation occurs when micrometeorites hit a body's surface and a certain volume of the regolith is vaporised and released into the exosphere. The process is simulated in exact analogy to thermally released particles: The Maxwellian distribution in this case is driven by an average gas vapour temperature of 4000 K (Wurz and Lammer, 2003 and references therein).

Since the knowledge about velocity and size distributions of the micrometeorite flux in the asteroid belt is limited, we follow the procedure of Cintala (1992). He derived meteorite fluxes (in the mass range of 10^{-18} to 0.1 g) and vaporisation rates for the Moon and Mercury by scaling the meteorite flux on Earth. In general the amount of evaporated mass per unit area and time due to micrometeorite impact vaporisation can be found by (Bruno et al., 2006)

$$M_{\mathrm{vap}} = \rho_r \int_{v_{\min}}^{v_{\max}} \int_{\mu_{\min}}^{\mu_{\max}} f(v)h(\mu)V_{\mathrm{vap}}(v,\mu)\,\mathrm{d}v\,\mathrm{d}\mu, \tag{7}$$

where ρ_r is the density of the surface, $h(\mu)$ and $f(v)$ are the differential mass and velocity distribution, respectively, of the incident meteorites. V_{vap} describes the vaporised material of the regolith by an impacting spherical object of mass μ, velocity v and density ρ_p (Cintala, 1992),

$$V_{\mathrm{vap}} = \frac{\mu}{\rho_p}\left(c + dv + ev^2\right); \tag{8}$$

here c (-0.767), d (-0.0986 km^{-1} s) and e (0.0215 km^{-2} s^2) are constants dependent on the target temperature and the composition (Cintala, 1992; Table 3). We chose the values for a diabase projectile ($\rho_p = 3.012$ g cm^{-3}) into a regolith target ($\rho_r = 1.800$ g cm^{-3}) of temperature 273 K for our calculation. Cintala (1992) described the differential velocity distribution of meteorites in free space at heliocentric distance r as

$$f(v) = 3.81r^{0.2}\left(\frac{v}{\sqrt{rv^2 + v_{\mathrm{Ee}}}}\right)^3 e^{-0.247\sqrt{rv^2+v_{\mathrm{Ee}}}}, \tag{9}$$

where v_{Ee} is the escape velocity from Earth at 100 km altitude (11.1 km s^{-1}, coming from the observations of meteors on Earth). This velocity distribution can be corrected for gravitational focusing by the escape velocity of the considered body, which are in the case of asteroids, very small. Cintala (1992) assumes the mass distribution to be independent of the velocity distribution. Actually the function $h(\mu)$ was assumed to be the same for the Moon and Mercury. Since we do not know more about the mass distribution, we use this assumption also for the two asteroids. The function $h(\mu)$ is a polynomial expression and described in detail by Bruno et al. (2006); we do not repeat it here.

Solving the integral [Eq. (7)] with the given relationships, we found vapour production rates from impacting micrometeorites of masses between 10^{-18} and 0.1 g of 8.46×10^{-18} g cm^{-2} s^{-1} for (2867) Steins and 3.39×10^{-19} g cm^{-2} s^{-1} for (21) Lutetia. The reason for the considerably lower rate at Lutetia is the greater distance to the Sun and the therefore decreased mean impact velocity of 7.80 km s^{-1} compared to 8.79 km s^{-1} for Steins. Together with mean weights $\tilde{m}$ of regolith atoms, it is easily possible to derive flux rates from the surface into the exosphere for each species. The flux $\varphi_i^{\mathrm{meteor}}$ of released particles of species i by impact vaporisation can then be calculated as

$$\varphi_i^{\mathrm{meteor}} = \frac{M_{\mathrm{vap}}}{\tilde{m}}F_i; \tag{10}$$

here M_{vap} is given from Eq. (7). Note that this approach contains at least two uncertainties: First, the mass distribution was measured at Earth's orbit and is assumed to be the same in the orbit of the two asteroids; and second, Cintala (1992) assumed that the spatial density of particles varies with $r^{-1.3}$, as suggested by Leinert et al. (1981) for heliocentric distances from 0.3 to 1 AU, when r is the distance to the Sun. However, different dependences are reported: e.g. Mann et al. (2004) state that the distribution follows roughly r^{-1}. We use the same approach for distances of 2.14 and 2.72 AU as Cintala (1992) does. Since the asteroid belt may be a source of micrometeorites and dust, the spatial density and the mass distribution of the particles could vary substantially.

Together with the fluxes, described above [Eqs. (3), (5), and (10)], and Eq. (1), an exospheric surface density for each release process and species can be derived to scale the density profile of the exosphere from the numerical simulation. This procedure is implemented in the Monte Carlo code. The input parameters used to simulate the exospheres are therefore the relative abundance of each species F_i (composition) and some general parameters describing for example the orbital characteristics or the solar wind circumstances of each asteroid.

The majority of released particles are neutrals and since collisions can be neglected, the main process that can ionise the neutral contribution of an exosphere is photo-ionisation: Having photo ionisation rates and time steps, it is straight forward to calculate the amount of ionised species (released as neutrals) at every altitude above the exobase.

Table 1
Physical and orbital properties of (2867) Steins

Property	Value	Reference
Semimajor axis (AU)	2.364	Barucci et al. (2005)
Eccentricity	0.146	Barucci et al. (2005)
Inclination (deg)	9.944	Barucci et al. (2005)
Rotation period (h)	6.048 ± 0.007	Weissman et al. (2007)
Geometric albedo	0.45 ± 0.1	Fornasier et al. (2006)
Absolute magnitude	12.561	Barucci et al. (2005)
Slope parameter G	0.15*	Barucci et al. (2005)
Diameter (km)	4.6	Fornasier et al. (2006)

* Assumed by this authors for the calculation of the absolute magnitude above. Weissman et al. (2007) suggest a value of 0.4 to be more typical for E-type asteroids.

3. Properties and possible compositions

3.1. (2867) Steins

Discovered in 1969 by N. Chernykh, Asteroid (2867) Steins was not investigated in detail before it was selected as Rosetta flyby target in 2004. The main orbital and physical properties of (2867) Steins are listed in Table 1.

Recent investigations have increased the knowledge of the small asteroid: Based on the VIS and NIR spectrum (Barucci et al., 2005) and the high geometric albedo (e.g. Fornasier et al., 2006) it was classified as an E-type asteroid. This seems to be the general opinion, although Weissman et al. (2007) claim that the asteroid is unusually red for this taxonomic class.

E-type asteroids are thought to be differentiated bodies which suffered substantial heating. Probably these asteroids are the parent bodies of enstatite chondrites or enstatite achondrites (aubrites).

Barucci et al. (2005) compared two spectra of these meteorite types to spectra of (2867) Steins. They found that the enstatite chondrite Atlanta (EL6) presents a similar spectral behaviour, except for the spectral feature at about 0.5 μm. This feature could be produced by some sulfides. The aubrite ALH78113 presents similar spectral features like Steins, but with a flatter general behaviour at wavelengths larger than 0.6 μm. For our composition estimation we concluded that the aubrite would probably be a better choice to estimate the composition of Steins, because space weathering may make spectra redder, but the diagnostic parameters, like e.g. the absorption features, remain more or less unchanged, see e.g. Gaffey et al. (2002).

Clark et al. (2004) investigated spectra of E-type objects and used mixing models according to Hapke-theory to constrain possible surface compositions. They found, that the E-class may be divided into 3 smaller groups. (2867) Steins probably belongs to the Angelina, or E(II) group, as has already been suggested by Barucci et al. (2005). For our purpose we used the best mixing model results of the two simulated E(II) asteroids, (64) Angelina and (3103) Eger, from Clark et al. (2004) as volumetric ratios of the chosen end-members. At that time (2867) Steins was not yet classified as E-type asteroid. The reason for our choice is that the mixing models simulate optical properties of area mixtures. Area-ratios fit better with volume than with weight ratios. Elemental abundances can be obtained from this procedure using adequate densities for each end-member. Clark et al. (2004) were careful not to make any quantitative statements about the composition of any asteroid. However, we need elemental abundances as input for the model as they are listed in Table 2, but one must be aware that these are estimations and not exact determinations. Scaling the composition of Steins to a known grain density from a meteorite composition, a grain density (no voids) for the composition can be estimated.

Table 2
The elemental abundances (in wt%) for typical meteorites from the enstatite chondrite and aubrite type and the simulated E-type asteroids (64) Angelina and (3103) Eger, derived from Clark et al. (2004) and densities from the different end-members

	(64) Angelina	(3103) Eger	Enstatite chondrite	Aubrite	(2867) Steins
O	46.65	45.24	31.00	46.31	44.04
Na	0.62	0.59	0.58	0.15	0.58
Mg	20.45	19.97	13.75	22.49	20.04
Al	1.39	1.34	1.00	0.48	1.00
Si	26.88	26.00	18.80	26.88	25.41
P	0.00	0.00	0.13	0.01	0.12
S	1.35	2.63	3.10	0.49	1.78
K	0.04	0.04	0.07	0.02	0.07
Ca	2.10	3.69	1.02	0.61	1.02
Ti	0.02	0.02	0.06	0.03	0.05
Cr	0.01	0.01	0.30	0.02	0.30
Mn	0.01	0.01	0.16	0.03	0.16
Fe	0.54	0.51	24.80	4.11	3.88
Ni	0.00	0.00	1.47	0.06	1.47
Co	0.00	0.00	0.07	0.01	0.07
Total	100.06	100.05	96.30	101.70	100.00

Notes. The estimated composition of Steins is more or less similar to that of the aubrite and was derived by weighting the different possible compositions, bearing in mind the differences from the discussion above. Data for the EL Meteorite were taken from Lodders and Fegley (1998, Table 16.11). Data for the aubrite are from Watters and Prinz (1979, Table 13).

Table 3
Physical and orbital properties of (21) Lutetia

Property	Value	Reference
Semimajor axis (AU)	2.435	Barucci et al. (2005)
Eccentricity	0.164	Barucci et al. (2005)
Inclination (deg)	3.064	Barucci et al. (2005)
Rotation period (h)	8.17 ± 0.01	Barucci et al. (2005)
Geometric albedo	0.208 ± 0.025	Mueller et al. (2006)
Absolute magnitude	7.294	Barucci et al. (2005)
Slope parameter G	0.110	Barucci et al. (2005)
Diameter (km)	98.3 ± 5.9	Mueller et al. (2006)

3.2. (21) Lutetia

With a diameter of roughly 100 km, as confirmed by several authors (see Mueller et al., 2006), (21) Lutetia is the largest asteroid of the possible Rosetta flyby targets. Physical and orbital characteristics of (21) Lutetia are given in Table 3. Lutetia was classified as M-type asteroid by several authors in the late 80s and early 90s (for a short overview see Barucci et al., 2005). The reason for this classification was the high IRAS (In-

Table 4
Elemental abundances (in wt%) for typical meteorites of the CO and CV type

	Vigarano	CV	CO	(21) Lutetia
O		37.00	37.00	37.16
Na		0.34	0.42	0.34
Mg	13.79	14.30	14.50	14.36
Al	1.75	1.68	1.40	1.69
Si	14.99	15.70	15.80	15.77
P	0.11	0.11	0.12	0.11
S		2.20	2.20	2.21
Ca	1.86	1.84	1.58	1.85
Ti	0.09	0.09	0.07	0.09
Cr	0.33	0.35	0.35	0.35
Mn	0.14	0.15	0.16	0.15
Fe	21.81	23.50	25.00	23.60
Ni	1.44	1.32	1.42	1.33
H		0.28	0.07	0.28
C		0.53	0.44	0.53
H2O		0.15	0.20	0.15
K		0.04	0.04	0.04
Total	56.30	99.58	100.77	100.00

Notes. The estimated composition for Lutetia is similar to that of the CV composition, since all three abundances are more or less the same. Data for the Vigarano meteorite were taken from Wolf and Palme (2001, Table 9) and are listed for comparison. Other abundances are from Lodders and Fegley (1998, Table 16.11) and are comparable to other average compositions (e.g. Wolf and Palme, 2001, Tables 9 and 10) for those elements listed in both publications.

frared Astronomical Satellite) albedo of 0.221 ± 0.020 which was confirmed by Mueller et al. (2006) who reported a value of 0.208 ± 0.025. Already in the mid-90s observations showed that the infrared spectrum was unusually flat for a parent body of iron meteorites. Birlan et al. (2004) found a similarity with the carbonaceous chondrites of the CV3 or CO3 type. They suggested that these types of chondrites are characterised by low carbon contents, which could explain the relative high albedo compared to other types.

Meanwhile many other observational results are in agreement with the assertion of a primitive surface composition of (21) Lutetia: Polarimetric properties, lower radar albedo, and an absorption feature at 3 μm diagnostic of water of hydration (Barucci et al., 2005 and references therein). A shallow water band around 3 μm was also reported by Birlan et al. (2006).

In conclusion no certain taxonomic classification of (21) Lutetia is available, although most recent studies tend to be consistent with the C-type classification. For the reasons mentioned above, we assume for this simulation that Lutetia's surface composition is similar to that of CO3 or CV3 meteorites, in particular to that of the Vigarano meteorite, as suggested in Barucci et al. (2005). For comparison of the different compositions see Table 4.

4. Input parameters

The encounter of Rosetta with (2867) Steins and (21) Lutetia will be at a heliocentric distance of 2.14 and 2.72 AU, respectively. We used the solar constant of $S_0 = 1380\,\mathrm{W\,m^{-2}}$, integrated UV photon flux of $3.31 \times 10^{15}\,\mathrm{cm^{-2}\,s^{-1}}$ (Wurz and Lammer, 2003), and a typical solar wind ion flux of $4 \times 10^{12}\,\mathrm{m^{-2}\,s^{-1}}$ in Earth's orbit, which we scaled according to r^{-2}. The solar wind speed was assumed to be $400\,\mathrm{km\,s^{-1}}$.

From the vapour production rate due to impacts of micrometeorites a mean particle release rate of 8.45×10^8 and $9.11 \times 10^7\,\mathrm{m^{-2}\,s^{-1}}$ for Steins and Lutetia were derived, respectively.

The bolometric bond albedo A_b was derived from the geometric albedo and the phase integral q, which is calculated with the slope parameter G and the relation given from the H, G magnitude system described by Bowell et al. (1989)

$$q = 0.290 + 0.684G. \tag{11}$$

For Steins we used a typical value of $G = 0.4$, as suggested by Weissman et al. (2007).

For the emissivity ε a typical value of 0.9 was taken. We did not take into account any possible correction of the beam factor η to calculate the temperature of the subsolar point.

Probably the hardest thing to estimate are the masses of each asteroid. Mass is important since it determines gravitational acceleration, escape velocity and the Hill radius, which need to be known to track a released particle. We derived possible densities by scaling known meteorite analogue grain densities to the estimated compositions of each asteroid. The bulk density of asteroids can differ from grain densities since asteroid porosities might be as high as 70%. For example, the NEAR Shoemaker target (243) Mathilde, a C-type asteroid, showed an extremely low density of only $1.3 \pm 0.2\,\mathrm{g\,cm^{-3}}$, which probably can be explained with high porosity (Veverka et al., 1999).

Britt et al. (2002) estimated total porosities of asteroids with known masses by scaling the bulk density of the asteroid by the grain density of its best meteoritic spectral analogue. We assumed for both Rosetta targets a total porosity of 40%: This value seems to be a good average of all estimated asteroid porosities, in particular of the C-type asteroids.

In this manner we derived bulk densities for (2867) Steins and (21) Lutetia of 2.305 and $2.443\,\mathrm{g\,cm^{-3}}$, respectively. Note that these values compare well with other asteroid densities derived using different techniques (e.g. Britt et al., 2002). However, an exact determination of the densities of Steins or Lutetia is not possible with the existing data. The slightly higher estimated bulk density for Lutetia comes from the higher abundance of iron in the CV meteorites compared to the enstatite types.

The total porosity includes both micro- and macroporosity, and it is also used to reduce the surface density of e.g. the sputter contribution of certain species. The surface of an asteroid is not solid but covered by a layer of regolith. This is probably also true for small asteroids like Steins, since the Hayabusa target Itokawa shows evidence of cm to mm sized regolith existing on its surface (Fujiwara et al., 2006). Itokawa, with major axes of $535 \times 294 \times 209$ m, is clearly smaller than Steins, nevertheless it is able to retain small particles on its surface. However, Itokawa may be a rubble pile and therefore (2867) Steins may show different behaviour in some points. The exospheric surface densities are reduced thus solar wind ions or UV photons penetrate the surface and any ejected particles are not necessarily introduced into the exosphere but may remain within the

Table 5
Species-independent input parameters used for the Monte Carlo simulation

	(2867) Steins	(21) Lutetia
Heliocentric distance r (AU)	2.14	2.72
Solar radiation flux (W m^{-2})	301	187
Solar wind ion flux (m^{-2} s^{-1})	8.73×10^{11}	5.41×10^{11}
Solar wind velocity (km s^{-1})	400	400
UV photonflux φ_{photon} (m^{-2} s^{-1})	7.23×10^{18}	4.47×10^{18}
Particle flux from meteorites (m^{-2} s^{-1})	8.45×10^{8}	9.11×10^{7}
Phase integral q	0.5636	0.3652
Bolometric bond albedo A_b	0.2536	0.0760
Beam factor η	1	1
Emissivity ε	0.9	0.9
Subsolar temperature T_{ss} (K)	258	241
Grain density (kg m^{-3})	3227	3420
Bulk porosity	0.40	0.40
Bulk density (kg m^{-3})	2305	2443
Volume (m^3)	5.10×10^{10}	4.97×10^{14}
Mass (kg)	1.17×10^{14}	1.22×10^{18}

Note. For more information see text.

regolith. Although the surface porosity may be higher than the bulk porosity, we use the same value for both of these properties.

Together with the diameter, the density leads to a mass estimate for the two asteroids, which can be used to follow the trajectory of each released particle. For both asteroids a spherical shape was assumed and the calculations were done for the subsolar point, where we expect the highest surface densities of the exospheres. Table 5 summarises the input parameters for the simulations.

We would like to point to the fact that the knowledge about the two asteroids originates mainly from observations in the visible and near infrared wavelength range. These wavelengths can only probe the uppermost layer of an asteroid's regolith. Even radar techniques are not able to investigate most of the internal structure of such bodies. The composition estimate and the derived bulk densities, which are used to calculate parameters such as the masses, underlie the constraining assumption, that the asteroid surface is representative for the whole asteroid. On the other hand, the mechanisms of sputtering and impact vaporisation will produce an exosphere which represents more or less the surface composition. In conclusion, this assumption is only necessary to estimate some physical parameters (like mass or the escape velocity) of each asteroid.

5. Results

5.1. (2867) Steins

We let the model run with an appropriate resolution (meaning in this case a small step size) for 100,000 released particles per species to ensure good statistics. Figs. 1 and 2 show the results for the smaller asteroid (2867) Steins and the different release processes. Note that all calculations were done for the subsolar point. For reasons of clarity only the most important species were drawn.

Steins is obviously too small to hold back many particles: Above a distance h of roughly 10 km all density profiles show a h^{-2} behaviour. Since all particle velocities exceed the estimated escape velocity, this is not surprising.

Note that the density profiles of solar wind sputtering are not highly stoichiometric on a short time scale: The introduced binding energy differs for the different species. As an example, in our model Mg is sputtered clearly more efficiently than Si due to a lower surface binding energy. This procedure will lead to a depletion of elements with lower surface binding energies in the top-most surface layers and, on the other hand, in an enrichment of those with higher binding energies. This process continues until an equilibrium is achieved where the sputter yields represent the bulk composition of the solid. This process is well understood from laboratory experiments (Betz and Wehner, 1983) but we do not simulate that effect.

In contrast, micrometeorite impact vaporisation releases a certain volume at once and this volume might represent the surface composition better. In our model, we find that the contribution of solar wind sputtering is about one order of magnitude higher than impact vaporisation at the subsolar point.

If one assumes a constant sputter yield, that means a reduction of the released particle flux only due to the cosine dependence of solar wind ion flux with lower zenith angle, the average exospheric surface density of the hemisphere facing the Sun is a factor of 2 smaller than the density at the subsolar point. On the other hand, micrometeorite impact vaporisation is not coupled to the Sun direction and the resulting surface densities are more or less the same at every location. Since the average surface densities from sputtering are higher than those from impact vaporisation, our model suggests that on the sunlit hemisphere sputtering is the process that releases most of the refractory elements. From the average surface density and the release velocity we estimated a global release rate of 6.84×10^{17} s^{-1} for sputtered oxygen compared to 3.27×10^{16} s^{-1} for oxygen released by impact vaporisation. On the night side, impact vaporisation is clearly dominant because Sun-driven processes cease. However, we want to stress again that the vapour production rate due to micrometeorites contains uncertainties which could influence the contribution of impact vaporisation on the Sun side.

Quantitatively the sodium released by photon stimulated desorption seems, according to this model, to exceed all the other species by about one order of magnitude. Although PSD is not an easily simulated release process, the resulting density profile of sodium can be viewed as a reliable estimate since Wurz and Lammer (2003) were able to reproduce some observations of Mercury's sodium exosphere quite well. However, uncertainties in the abundance of sodium in the surface regolith of any asteroid remain. Since neutral sodium exhibits strong transition lines in the visible wavelength range it is therefore well observable even in rather small abundances the column density might be of interest. We found a total zenith column density of 5.64×10^{10} m^{-2}, which is clearly exceeded in the sodium exospheres of Mercury (2×10^{11} cm^{-2}) and the Moon ($0.5–2 \times 10^{9}$ cm^{-2}), see Killen and Ip (1999).

Only solar wind species, He and H, might have higher densities than Na. For the calculation of these species we assumed an input–output equilibrium, which is not very realistic for the

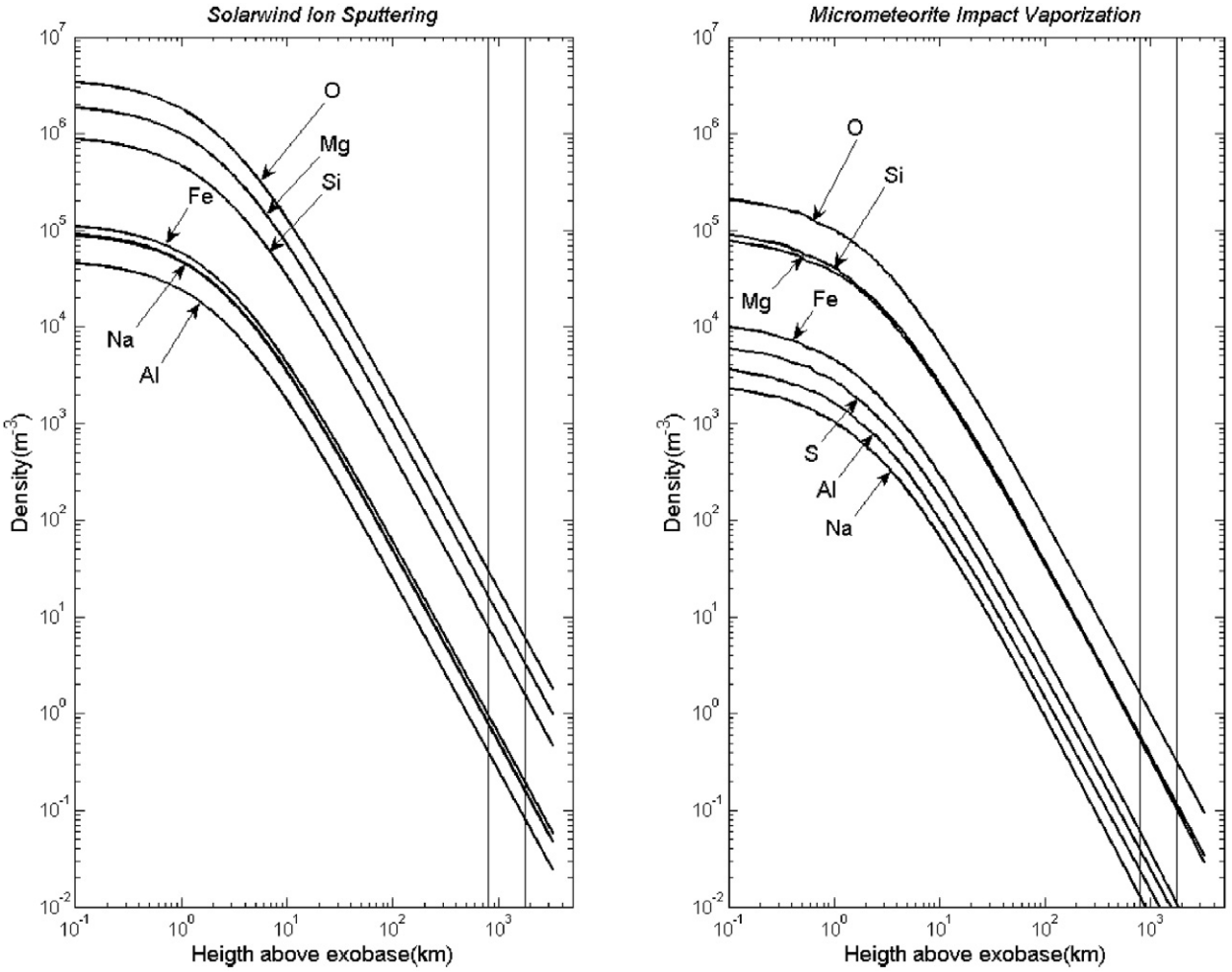

Fig. 1. Calculated density profiles for (2867) Steins from solar wind sputtering (left panel) and micrometeorite impact vaporisation (right panel). The density profile of sulfur from sputtering lies behind the one of sodium. The vertical black lines show the range of Rosetta's closest approach (between 800 and 1800 km). For details see text.

subsolar point, but for the whole asteroid. The surface densities of He and H therefore probably have to be reduced. Furthermore, solar wind protons are reactive and may cause chemical sputtering as soon as they are implanted in the surface regolith. Chemical sputtering of solar wind H on silicates could be a source of H_2O molecules, which could be bound by the surface or be released into the exosphere too (e.g. Potter, 1995). Other possible exogenous sources of H_2O are impacting meteorites and dust. Some E-type asteroid may show water-of-hydration absorption features (Clark et al., 2004 and references therein) in their spectra, but since, to our knowledge, nothing is reported about a similar behaviour of (2867) Steins, we are careful in assuming these species in the exosphere. In conclusion, the density profile of He and H have to be viewed as an upper limit.

During closest approach, we expect particle densities of the most abundant sputtered species in the range of 10–100 particles per m^3, which is somewhat lower than for sodium, released by PSD. Most of the particles are neutrals, since the ionisation rate is low: For potassium released by PSD, which is according to this model the most ionised species, of all released neutral K only 8.1% were ionised on their way to 5000 km altitude. For sodium the ionised fraction of the neutrals are for sputtering 0.9%, for PSD 5.0% and for impact vaporisation 5.4%. These numbers make clear which processes are more energetic than others: Fast particles are ionised less likely than slow particles. For most of the other species shown in Figs. 1 and 2, the ionised fraction of neutrals is less than 1%.

5.2. (21) Lutetia

The results for the bigger asteroid (21) Lutetia, shown in Figs. 3 and 4, are in general similar to those of (2867) Steins.

It is obvious that Lutetia has by far a larger exospheric density than Steins: The density profiles have a flatter trend up to roughly one asteroid radius above the surface. Then again, a spherical decrease of the density becomes visible. However, Lutetia is still not heavy enough to discriminate different masses: Heavier species are not bound much stronger than lighter species. A slight, but not overwhelming difference can be seen when looking at the numerical results in detail.

In addition, practically all released particles escape from the asteroid: e.g. 99.87% of all thermally released H_2O molecules escape from the asteroid. For all other species, the rate is even higher. With a surface density of roughly 10^7 m^{-3}, desorbed

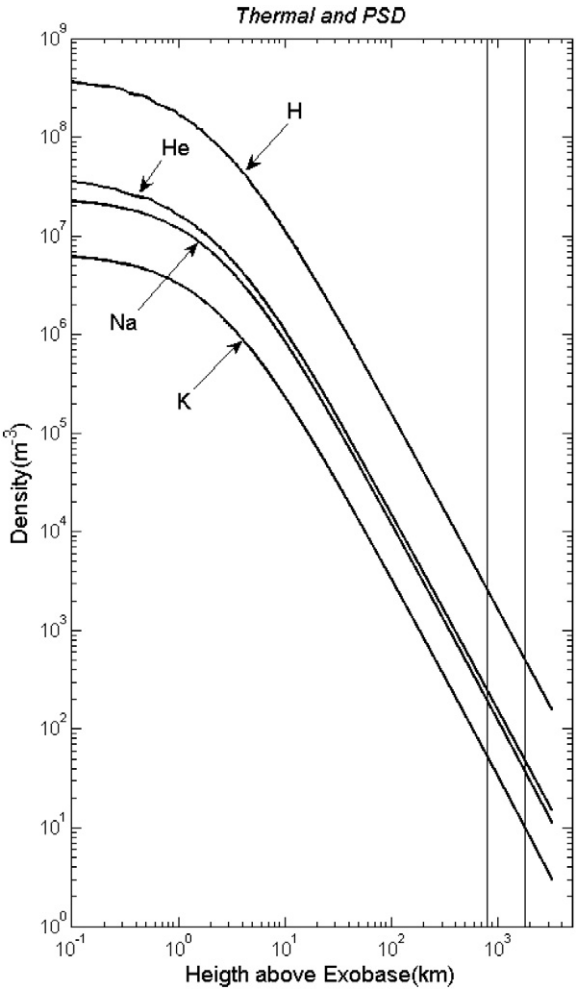

Fig. 2. Calculated density profiles for (2867) Steins from thermally released solar wind species and Na and K from PSD. For details see text.

sodium is again about one order of magnitude higher than oxygen from solar wind sputtering. This is equivalent to a zenith column density of 4.51×10^{11} m^{-2} or roughly 2% of the observed zenith column density of sodium in the lunar exosphere (Killen and Ip, 1999). The total release rate for sputtered oxygen on the sunlit hemisphere is about 1.64×10^{20} s^{-1} and for impact vaporisation the global loss is 1.44×10^{18} s^{-1}.

In Fig. 4, the difference of the slope of the density profile from sodium and e.g. He close to the asteroid's surface, has its origin in the different release processes: The angular distribution of thermally released particles is modelled with a 3-dimensional Gaussian distribution, which is broader than the cosine squared distribution we assumed for the polar angle of photon stimulated desorption. In other words the released sodium is pointed in a narrower solid angle and the density falls off less rapidly.

During the Rosetta encounter, Lutetia is further away from the Sun than Steins. Therefore, the ionisation rate is even smaller: The most ionised species in an altitude of 5000 km is calcium from impact vaporisation with an ionised fraction of roughly 11.6%. A similar behaviour can also be expected for Ca in Steins' exosphere, but the estimated calcium abundance there is almost a factor of 2 lower than in Lutetia's regolith (Table 2). However, the exospheric Ca densities are rather low compared to other species.

Since Lutetia may be a carbonaceous chondrite parent body, it supports the hope of bearing more volatiles than (2867) Steins. Table 4 shows that CO and CV meteorites contain a small amount of water. We let the model run for this species and estimated a exospheric surface density of 10^6 m^{-3}. The release rate of water is of course somehow speculative, but recent work revealed that some main belt asteroids show comet-like behaviour: Hsieh and Jewitt (2006) observed that some asteroids with semimajor axis around 3.2 AU exhibit outbursts due to subsurface ice.

Although most exospheric surface densities are lower (due to the increased heliocentric distance), at the closest approach we expect densities of about one order of magnitude higher than for (2867) Steins.

6. Conclusions

Our results suggest that solar wind sputtering is the most important exospheric supply process on the sunlit side of an asteroid. The most abundant species in the asteroidal exosphere are the most abundant refractory elements in the surface regolith. Exceptions might be the sodium released very efficiently by PSD and implanted solar wind ions. The majority of released particles are neutrals, since the dominant release processes are ion sputtering and photon stimulated desorption.

We found that for Lutetia and Steins, photo-ionisation is too weak to ionise a reasonable quantity of released atoms until they reach the altitude of closest encounter from Rosetta.

For (2867) Steins volatiles are probably not a good opportunity for an investigation by mass spectrometers, since recent observations point to a thermally active history. Neutral oxygen or sodium may present the best chances for a successful measurement at this small asteroid, although the expected densities at the distance of closest encounter are very low.

(21) Lutetia is considered to be a more primitive asteroid, where thermal release could also play an important role. However, the discussion about the meteorite analogue, on which this work is based, is probably not yet finished. In particular, there is still the unusual high albedo that is not typical for carbonaceous chondrites. Other candidates are, in analogy to (2867) Steins, neutral oxygen or sodium, where ROSINA has clearly better chances to make a successful measurement than in the surrounding of the first Rosetta flyby target.

The major advantage of the adaptation of this model for asteroids is that no assumptions about the exospheres are necessary. The model includes all the surface-processes and therefore necessary estimations can at least be compared to some observational or experimental data (e.g. the surface composition with meteorites, the bulk density with known masses of other asteroids, etc.). Furthermore it is obvious that the simple assumption of a spherical decreasing density profile would lead to significant lower densities than our model suggests. Since our primary goal was to determine quantitative densities, and

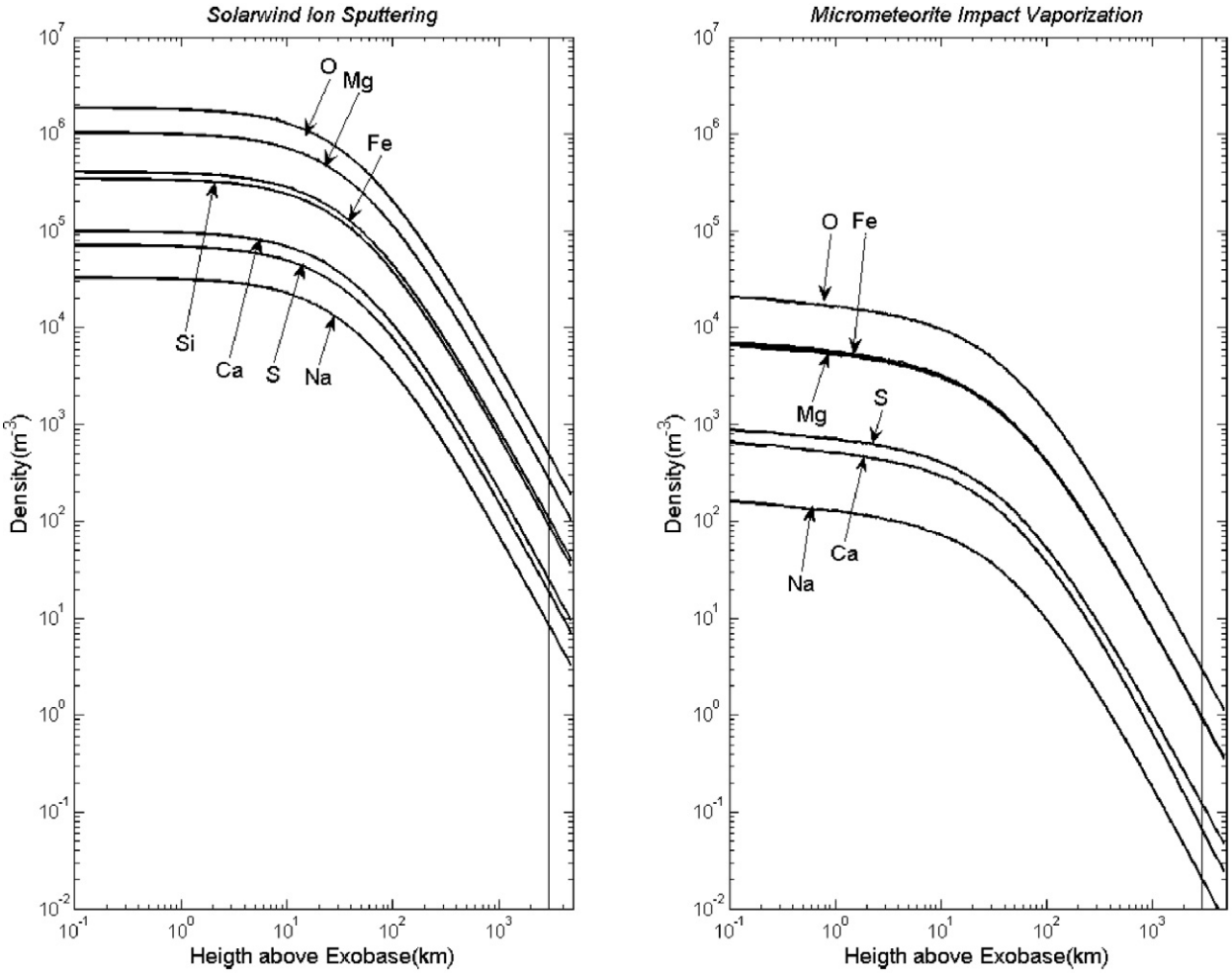

Fig. 3. Calculated density profiles for (21) Lutetia from solar wind sputtering (left panel) and micrometeorite impact vaporisation (right panel). The density profile of silicon from impact vaporisation is overlaid by the ones of iron and magnesium. The vertical black line shows the range of Rosetta's closest approach (300 km). For details see text.

little is known about exospheres of asteroids, the adaptation of an existing model has to be preferred to any other approach.

In this simulation we did not take into account several species, which are very likely existent in an asteroid's regolith and therefore may also be present in the exosphere. One example are noble gases: Typical abundances of noble gases in meteorites are in the order of ppb to ppm weight fraction. Since the asteroid belt may be the main source of meteorites, we do not see a reason, why asteroids should contain more noble gases. These, probably trapped noble gases, would have to be released by for instance significant heating.

One way to estimate such noble gas fluxes from an asteroid's surface is to apply the processes of sputtering and impact vaporisation stoichiometrically to the noble gas species. This yields surface densities which are lower than those shown in Figs. 1–4 by several orders of magnitudes. We therefore doubt that noble gases may be measurable species in the exosphere of any asteroid.

For impact vaporisation of micrometeorites, we did not take into account the contribution of the projectiles to the vapour production rate. Since meteorite impact velocities in our model are small, the mass of vaporised regolith is roughly in the same order of magnitude like the projectile itself (for comparison see Cintala, 1992; Fig. 5). Since the exospheric supply from impact vaporisation is highly uncertain due to the unknown flux of meteorites, the contribution of the projectiles seems to be unimportant at the moment. The uncertainty of the impact vaporisation contribution to the exosphere does not matter for our purposes, because impact vaporisation and solar wind sputtering release the same species.

Refractory elements, which are also existent in the solar wind in very small amounts, are also not included in the calculation of the sputtering contribution described above. These refractory elements may be implanted in an asteroids surface and may induce a compositional change. Heavy ions make up roughly 0.1% (Wurz et al., 2007) of the solar wind flux, which in case for Lutetia corresponds to an incident ion flux of about 5.4×10^8 m^{-2} s^{-1}. Since a typical sputter yield is 0.1, the removed particles exceed this flux by a factor of about 100. This is enough to get rid of solar wind implanted heavy ions.

The ROSINA instrumentation package consists of two complementary mass spectrometers, the Double Focusing Mass Spectrometer (DFMS) and the Reflectron Time of Flight instrument (RTOF), and a pressure sensor (COPS). DFMS is de-

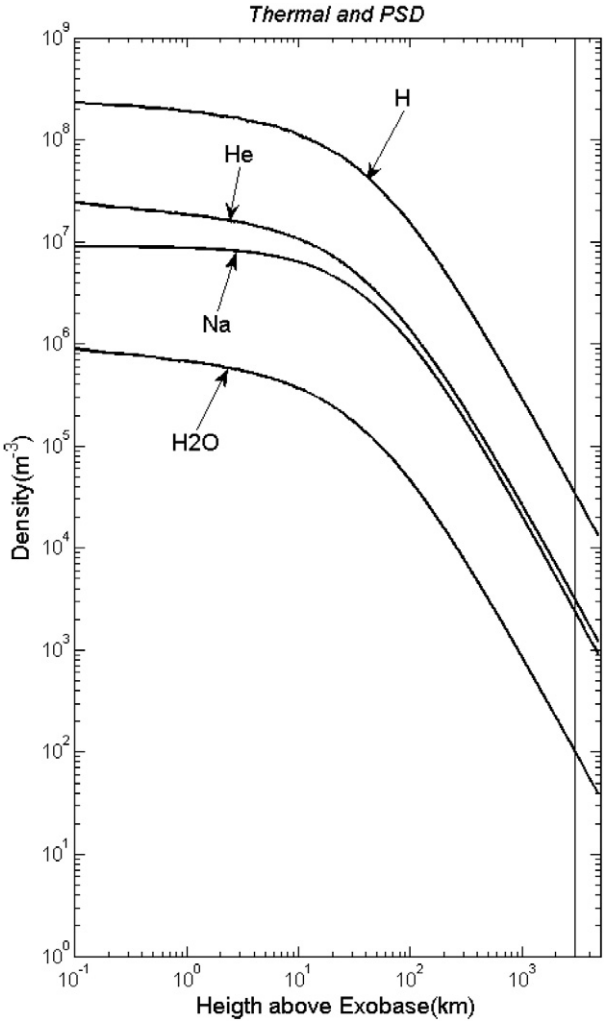

Fig. 4. Calculated density profiles for (21) Lutetia from thermally released solar wind species and Na from PSD. For details see text.

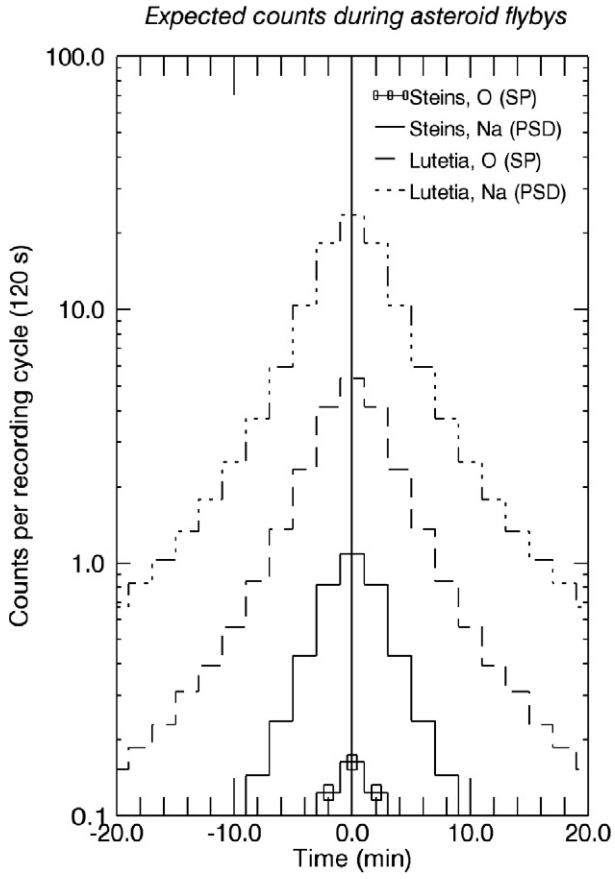

Fig. 5. Expected counts per recording cycle (120 s) of the DFMS sensor during the assumed flyby-scenarios. Time 0.0 min corresponds to the moment of closest approach. The numbers of expected counts are rather low for oxygen and sodium during the (2867) Steins flyby. However, during the (21) Lutetia flyby, the detected events should exceed the variations of a baseline measurement obtained prior or after the encounter. The abbreviation PSD refers to densities obtained by the photon stimulated desorption process, SP to particle sputtering.

signed for high mass resolution (3000 at 1% peak height) in the mass range of 12 to 150 amu. RTOF has high sensitivity for the mass range of 1 to >300 amu. The mass resolution is 500 at 1% peak height. For a detailed description see Balsiger et al. (2007). The primary scientific goal of the ROSINA instrument is to determine the composition of the ionosphere and atmosphere of the final ROSETTA target 67P/Churyumov–Gerasimenko. However, during the asteroid flyby's, the exospheres of these bodies will be investigated for the first time by means of mass spectrometry.

Although the detailed flyby scenarios are not known at present, we tried to calculate how many counts we expect during the two asteroid flybys. We assumed that the closest approach will be above the subsolar point and that the flight direction is perpendicular to the asteroid–Sun axis. Having number densities at the closest approach [800 km and 3000 km above surface for (2867) Steins and (21) Lutetia] and relative flyby velocities [8.6 km s^{-1} at (2867) Steins and 15 km s^{-1} at Lutetia, see Barucci et al., 2005] we can calculate the particle density profile along the ROSETTA trajectory. We expect that the number density within the sources of the sensor will be increased by roughly one order of magnitude since the neutrals are piled up due to the high flyby velocities. We estimate that for DFMS the number of events detected during the asteroid flyby is about 110 for sodium and 20 for oxygen at (21) Lutetia with the exosphere densities derived from our model. For (2867) Steins the numbers are about a factor 25 lower. These numbers are rather low but still within the capabilities of ROSINA (see Fig. 5), at least for Lutetia. However, there is enough time prior to the encounter as well as after the encounter to establish a good baseline and the performance of ROSINA is very stable as long as the thermal environment does not change drastically. This should allow us to detect single counts.

The time-dependence of the expected counts for the two flybys is shown in Fig. 5. The integration time was assumed to be 120 s for this calculation, as is typical for the ROSINA sensors. According to our model, it should be possible to detect the oxygen and sodium exosphere of (21) Lutetia, while a detection during the (2867) Steins flyby, where the integrated counts do not exceed 1 count per 120 s, is in question.

Under these circumstances it might look attractive to measure ions, since the sensitivity for ions is in general increased compared to neutrals. However, due to the high relative flyby

velocity the energy of the ions is about 20 eV whereas the ROSINA instruments are optimised for thermal ion energies (<10 eV). This reduces the sensitivity of the sensors considerably. Furthermore, it is expected that the boresight axis will be pointed to the asteroid during the flyby because of the camera operations. The ions would therefore enter the sensor with a non-negligible angle away from the ion-optical axis which will further decrease the instrument sensitivity. This effect is much less pronounced for neutrals for geometrical reasons.

With the many uncertainties of our model and the many unknowns of the asteroids it is certainly worthwhile to operate the ROSINA sensors during the asteroid flybys. In the best case we can derive a density profile (with limited space resolution), in the worst case we get a sensitive upper limit of the exosphere densities of the two asteroids.

The exospheres of asteroids are in particular interesting in respect of possible asteroid comet transitions: Observations showed that (1) Ceres exhibits escaping water (A'Hearn and Feldman, 1992) and, as mentioned above, several smaller asteroid's show comet-like outbursts (Hsieh and Jewitt, 2006). It may now be interesting to investigate if more primitive objects, which show (so far) no evidence for sublimation of ice, contain a significant endogenous water source. Furthermore, the observation of a possible sodium exosphere could be good evidence for the suggestions that an asteroids exosphere can be viewed as a transition between a thin planetary exosphere (like on Mercury) and a cometary coma, where the escape velocity is exceeded by practically all released particles. In both cases, Mercury and comets, the existence of either a sodium exosphere or tail is established. Moreover, even if a body is altered since its formation and there is little or no outgassing of volatiles, the investigation of the exosphere may reveal useful information about the surface composition.

The upcoming asteroid flyby's of the ROSETTA spacecraft will be the next possibility to investigate asteroids and their exospheres: In September 2008 the first E-type asteroid flyby will take place. Two years later the possibly more primitive object (21) Lutetia can be investigated. Finally, just about now the DAWN mission is in its starting blocks: This spacecraft will be sent to the Asteroids (4) Vesta and (1) Ceres, where it is also expected to detect possible exospheres (Russel et al., 2004).

References

A'Hearn, M.F., Feldman, P.D., 1992. Water vaporization on Ceres. Icarus 98, 54–60.

Balsiger, H., and 49 colleagues, 2007. Rosina–Rosetta Orbiter Spectrometer for ion and neutral analysis. Space Sci. Rev. 128, 744–801.

Barucci, M.A., Fulchignoni, M., Fornasier, S., Dotto, E., Vernazza, P., Birlan, M., Binzel, R.P., Carvano, J., Merlin, F., Barbieri, C., Belskaya, I., 2005. Asteroid target selection for the new Rosetta Mission baseline. Astron. Astrophys. 430, 313–317.

Betz, G., Wehner, G.K., 1983. Sputtering of multicomponent materials. In: Behrisch, T. (Ed.), Sputtering by Particle Bombardment II. Springer-Verlag, Berlin, pp. 11–90.

Biersack, J.P., Eckstein, W., 1984. Sputtering of solids with the Monte Carlo program TRIM.SP. Appl. Phys. A 34, 73–94.

Birlan, M., Barucci, M.A., Vernazza, P., Fulchignoni, M., Binzel, R.P., Bus, S.J., Belskaya, I., Fornasier, S., 2004. Near-IR spectroscopy of Asteroids 21 Lutetia, 89 Julia, 140 Siwa, 2181 Fogelin and 5480 (1989YK8), potential targets for the Rosetta Mission; remote observations campaign on IRTF. New Astron. 9, 343–351.

Birlan, M., Vernazza, P., Fulchignoni, M., Barucci, M.A., Descamps, P., Binzel, R.P., Bus, S.J., 2006. Near infra-red spectroscopy of the Asteroid 21 Lutetia. Astron. Astrophys. 454, 677–681.

Bowell, E., Hapke, B., Domingue, D., Lumme, K., Peltoniemi, J., Harris, A.W., 1989. Application of photometric models to asteroids. In: Binzel, R.P., Gehrels, T., Matthews, M.S. (Eds.), Asteroids II. University of Arizona Press, Tucson, pp. 524–556.

Britt, D.T., Yeomans, D., Housen, K., Consolmagno, G., 2002. Asteroid density, porosity, and structure. In: Bottke, W.F., Cellino, A., Paolicchi, P., Binzel, R.P. (Eds.), Asteroids III. University of Arizona Press, Tucson, pp. 485–500.

Bruno, M., Cremonese, G., Marchi, S., 2006. Neutral sodium atoms release from the surface of the Moon induced by meteoroid impacts. Mon. Not. R. Astron. Soc. 367, 1067–1071.

Cassidy, T.A., Johnson, R.E., 2005. Monte Carlo model of sputtering and other ejection processes within a regolith. Icarus 176, 499–507.

Cintala, M.J., 1992. Impact-induced thermal effects in the lunar and mercurian regoliths. J. Geophys. Res. 97 (E1), 947–973.

Clark, B.E., Bus, S.J., Rivkin, A.S., McConnochie, T., Sanders, J., Shah, S., Hiroi, T., Shepard, M., 2004. E-type asteroid spectroscopy and compositional modeling. J. Geophys. Res. 109, doi:10.1029/2003JE002200. E02001.

Fornasier, S., Belskaya, I., Fulchignoni, M., Barucci, M.A., Barbieri, C., 2006. First albedo determination of 2867 Steins, target of the Rosetta Mission. Astron. Astrophys. 449, L9–L12.

Fujiwara, A., and 21 colleagues, 2006. The rubble-pile Asteroid Itokawa as observed by Hayabusa. Science 312, 1330.

Gaffey, M.J., Cloutis, E.A., Kelley, M.S., Reed, K.L., 2002. Mineralogy of asteroids. In: Bottke, W.F., Cellino, A., Paolicchi, P., Binzel, R.P. (Eds.), Asteroids III. University of Arizona Press, Tucson, pp. 183–204.

Hsieh, H.H., Jewitt, D., 2006. A population of comets in the main asteroid belt. Science 312, 561–563.

Hunten, D.M., Morgan, T.M., Shemansky, T.M., 1988. The Mercury atmosphere. In: Vilas, F., Chapman, C.R., Matthews, M.S. (Eds.), Mercury. University of Arizona Press, Tucson, pp. 562–613.

Killen, R.M., Ip, W.H., 1999. The surface-bounded atmospheres of Mercury and the Moon. Rev. Geophys. 37 (3), 361–406.

Leinert, C., Richter, I., Pitz, E., Planck, B., 1981. The zodiacal light from 1.0 to 0.3 A.U. as observed by the Helios Space Probes. Astron. Astrophys. 103, 177–188.

Lodders, K., Fegley, B., 1998. The Planetary Scientist's Companion. Oxford University Press, New York, pp. 290–331.

Mann, I., Kimura, H., Biesecker, D.A., Tsurutani, B.T., Grün, E., McKibben, R.B., Liou, J.-C., MacQueen, R.M., Mukai, T., Guhathakurta, M., Lamy, P., 2004. Dust near the Sun. Space Sci. Rev. 110, 269–305.

Mueller, M., Harris, A.W., Bus, S.J., Hora, J.L., Kassis, M., Adams, J.D., 2006. The size and albedo of Rosetta fly-by target 21 Lutetia from new IRTF measurements and thermal modeling. Astron. Astrophys. 447, 1153–1158.

Potter, A.E., 1995. Chemical sputtering could produce sodium vapour and ice on Mercury. Geophys. Res. Lett. 22 (23), 3289–3292.

Richter, I., Brinza, D.E., Cassel, M., Glassmeier, K.-H., Kuhnke, F., Musmann, G., Othmer, C., Schwingenschuh, K., Tsurutani, B.T., 2001. First direct magnetic field measurements of an asteroidal magnetic field: DS1 at Braille. Geophys. Res. Lett. 28 (10), 1913–1916.

Russel, C.T., and 20 colleagues, 2004. Dawn: A journey in space and time. Planet. Space Sci. 52, 465–489.

Veverka, J., and 13 colleagues, 1999. NEAR encounter with Asteroid 253 Mathilde: Overview. Icarus 140, 3–16.

Watters, T.R., Prinz, M., 1979. Aubrites: Their origin and relationship to enstatite chondrites. Proc. Lunar Sci. Conf. 10, 1073–1093.

Weissman, P.R., Lowry, S.C., Choi, Y.J., 2007. Photometric observations of Rosetta target Asteroid 2867 Steins. Astron. Astrophys. astro-ph/0702339v1.

Wolf, D., Palme, H., 2001. The Solar System abundances of phosphorus and titanium and the nebular volatility of phosphorus. Meteorit. Planet. Sci. 36, 559–571.

Wurz, P., Lammer, H., 2003. Monte-Carlo simulation of Mercury's exosphere. Icarus 164, 1–13.

Wurz, P., Rohner, U., Whitby, J.A., Kolb, C., Lammer, H., Dobnikar, P., Martin-Fernandez, J.A., 2007. The lunar exosphere: The sputtering contribution. Icarus 191, 486–496.

Ziegler, J.F., 2004. SRIM-2003. Nucl. Instrum. Meth. B 219, 1027–1036.